Ł. Sienkiewicz, R. Ryndzionek and M. Ronkowski, "Development of beltless respiration and heartbeat sensor based on flexible piezoelectric film," IECON 2019 - 45th Annual Conference of the IEEE Industrial Electronics Society, Lisbon, Portugal, 2019, pp. 784-789, doi: 10.1109/IECON.2019.8926827.

Development of beltless respiration and heartbeat sensor based on flexible piezoelectric film

1st Łukasz Sienkiewicz
Gdansk University of Technology
Faculty of Electrical and Control Engineering
Gdansk, Poland
lukasz.sienkiewicz@pg.edu.pl

2nd Roland Ryndzionek
Gdansk University of Technology
Faculty of Electrical and Control Engineering
Gdansk, Poland
roland.ryndzionek@pg.edu.pl

3rd Mieczysław Ronkowski
Gdansk University of Technology
Faculty of Electrical and Control Engineering
Gdansk, Poland
mieczyslaw.ronkowski@pg.edu.pl

***Abstract*—The main goal of this work is to report initial development on a respiration and heartbeat measurement sensor that can be used in continuous monitoring conditions at a minimal impact on the patient. General description of the sensor, consisting of a PVDF film and the bonding layer, is given. Open-circuit voltage generated by the sensor is estimated by analytical and numerical calculations. Analog and digital interface used to extract the bio-data is briefly described. Finally, signal conditioning with digital filters, as well as, measurements of respiration and heart rate at two locations are presented and discussed.**

***Index Terms*—sensor, piezoelectric, PVDF, measurements of respiration, heartbeat**

I. Introduction

The sensing and actuation characteristics of piezoelectric materials, the ability to generate and detect ultrasonic frequencies and the high potential of piezoelectric materials in smart systems make them well suited for medical diagnosis and therapy. Examples of applications for the piezoelectric phenomenon include, but are not limited to: tactile sensing for minimal invasive surgery, pace maker control, localized drug delivery, bone healing and measurement, and medical imaging [1].

Polymer films made of Polyvinylidene fluoride (PVDF) also possess the properties of piezoelectricity and pyroelectricity. PVDF became popular sensing material, due to features like high sensitivity, wide bandwidth, low acoustic impedance, good elasticity and low cost. It has been heavily investigated since its discovery in 1969. Research on monitoring of human physiological parameters with PVDF sensors is currently gaining momentum [2]–[4].

Among the physiological parameters respiration and heartbeat stand out as possessing key information on the health condition of the subject. In medical practice heart rate variability (HRV) is very important, treated as a non-invasive method of assessing the autonomic nervous system. The heart rhythm depends on the pressure (mainly due to the action of baroreceptor reflex), and the pressure depends on the heart rhythm, but both of these depend closely on the breath [5], [6].

Regular breath for a statistical healthy human is in the range of 12 to 20 bpm (breaths/min). On one hand, respiration rate (RR) of young athletic individuals is reported between 6 and 10 bpm. On the other hand, patients in the acute phase of a stroke often breathe over 30 bpm [7]–[9]. Apnoea is the most commonly occurring breath disorder. Obstructive sleep apnoea, for example, is a collapse of the airways at night, which causes more than 10 seconds-long interruptions of breathing. Such a situation poses higher cardiovascular risk [5].

Problems with measurement of respiration in clinical practice include: short registrations from the breathing belt, which records thoracic deformation, sensitivity to patient movements and conversation, as well as, lack of commonly available software to characterize breathing (regularity, periodicity, detection of characteristic patterns). Moreover, there are no specific parameters to assess the variability of breathing, apart from the existence of pauses and the assessment of RR [7]. Existing methods, such as polysomnography, acoustic or optic sensing, due to high costs, find limited use in the clinical settings [8].

The most frequently studied topics nowadays include wearable and unconstrained measurement systems. PVDF sensors can be placed on clothing, bed or chair. Some existing concepts include: sleep monitoring (detection of apnoea) with sensor matrix placed on the surface of bed or pillow; cantilever nasal sensors mounted on headphones, bending to an air flow from nostrils; sensor in patch form located near the upper lip, utilizing pyroelectricity to extract RR or pulse wave sensor located on the circumference of a steering wheel to detect drowsiness of the driver [10].

This work describes development process of a beltless respiration and heart rate sensor utilizing PVDF thin film. As opposed to belt or cantilever nasal sensors, the presented solution does not degrade the patient's comfort. Initial findings demonstrated in this paper, suggest that this sensor can be further developed into a system for continuous measurement in home conditions, instead of clinical surroundings. The paper is organized as follows: Chapter 2 gives general description of the sensor, its location and the bonding layer. In chapter 3 there is an analytical and numerical estimation of the charge and open-circuit voltage generated by the presented sensor. Next chapter describes the design of charge amplifier, ADC

and digital filters used to extract the bio-data. In chapter 5 measurements of respiration and heart rate at two locations are presented and discussed.

II. Description of the Sensor

The principle of sensor's operation is based on periodical deformations of a human body (chest wall or abdomen) during the physiological movements of respirations or vibrations generated by beating heart. Those mechanical deformations are driving the piezoelectric PVDF film so that electric charge appears on the electrodes, due to the direct piezoelectric effect. Electric output quantity is proportional to the mechanical stimuli and can be related to respiration rate (RR) or heart rate (HR).

The high sensitivity of PVDF as a receiver of mechanical work is obtained mainly due to the format of piezoelectric film material. The low thickness of the film makes a very small cross-sectional area, thus relatively small longitudinal forces create very large stresses within the material [3].

The PVDF film sensor used in this work was LDT1-028K manufactured by Measurement Specialties. The piezo-film element with silver ink electrodes is laminated to a sheet of polyester (Mylar), and produces a useable electrical signal output when forces are applied to the active area. The dimensions of the sensor, as well as basic material properties are given in Table I.

The sensor was placed on a subject's body in two locations: chest and abdomen area. Thanks to such an arrangement, it was possible to test the sensitivity in most popular placements of the sensor [10]. Secondly, location B gave the premise of simultaneous respiration and heartbeat rate measurements.

The sensor was attached thanks to a bonding layer. An elastic tape designed for rehabilitation purposes was used for this purpose. Its main characteristic was: stretching only in one direction (length - which corresponds with the respiration movements of the body), hypoallergenic, breathable and reusable. Basic sensor configuration, as well as measurement locations, are shown in Fig. 1.

TABLE I
Dimensions and basic material properties of the LDT1-028K PVDF sensor.

Property	Symbol	Model Value
Active length	l_p [mm]	30
Active width	w_p [mm]	12.19
Active Thickness	h_p [μm]	28
Capacitance	C_P [nF]	1.38
Strain constant	d_{31} [10^{-12} C/N]	23
Strain constant	d_{33} [10^{-12} C/N]	-33
Pyroelectric coefficient	p [10^{-6} KC/m^2]	30
Young's modulus	Y [10^8 N/m^2]	2 - 4
Relative permittivity	ϵ/ϵ_0 [-]	12 - 13
Mass density	ρ_m [10^3kg/m]	1.78

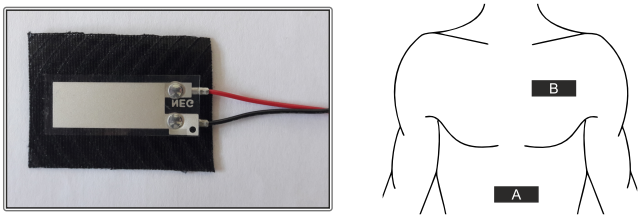

Fig. 1. PVDF piezoelectric sensor attached to a bonding layer (left); Placements of the sensor investigated in this work (right).

III. Estimation of Output Charge and Open-Circuit Voltage

A. Analytical

An electrical equivalent of the piezoelectric film element can be presented as either voltage source in series with a capacitance C_P, or a charge generator in parallel with a capacitance. The voltage source is the piezoelectric generator itself, which is directly proportional to the applied stimulus (pressure, strain, etc). Using constitutive equation we have:

$$D = dT + \epsilon E \tag{1}$$

Where D is electrical displacement, T is the mechanical stress, E is the electric field, d is the piezoelectric constant and ϵ is the permittivity. If a charge amplifier is used the electric field across the film is close to zero and term (1) is reduced to $D = dT$. The stress applied at the sensor's cross-section is:

$$T = \frac{F_b}{A} \tag{2}$$

Where: F_b is the applied force and A is the cross-section area ($A = w_p h_p$). The charge generated by the sensor can be calculated by integration over the loaded area:

$$q = \iint_A D dA = \iint_A dT dA = dTA = dF_b \tag{3}$$

Open-circuit voltage can be calculated thanks to D equal to zero in this state:

$$V_p = \frac{q}{C_P} = \frac{qt}{\epsilon A} = \frac{dF_b t}{\epsilon A} \tag{4}$$

LDT1-028K sensor produced open-circuit voltage of -1.82V between the electrodes, when load of F_b=0.1024 N or T=300 kPa was applied.

The low frequency limit of operation is defined by the greatest resistive load achievable, or by the largest capacitance load that still allows the signal to be easily detected. A piezoelectric sensor connected to a resistive load of R_L forms a high pass filter with cut-off frequency of:

$$f_p = \frac{1}{2\pi R_L C_P} \tag{5}$$

Sensor's operation in the low frequency range (fractions of Hz), reduction of cable's interface effects and adopting the output voltage to the levels safe for an ADC can be achieved using conventional charge amplifier.

B. Finite Element Analysis

The Finite Element Analysis (FEA) has been computed in ANSYS Workbench with piezoelectric and MEMS solver [11], [12], [13]. The simulation has been divided into two case-studies. Both are static simulations of piezoelectric film to determine the open-circuit voltage in response to the mechanical stimuli. Direction of force applied in each case is presented in Fig 2.

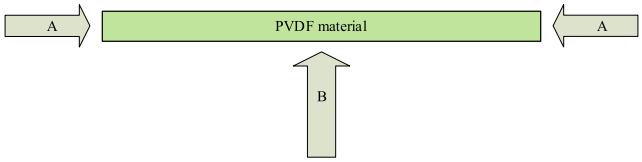

Fig. 2. Conditions of simulation for the static analysis.

The piezoelectric PVDF film has dimensions of 12x30x0.028 mm. The mesh settings have been adjusted to obtain an even distribution of finite elements. The mesh has been set as a adaptive size function, which resulted a 1664 elements and 12101 nodes. The convergence of results is very satisfactory. The mesh of finite elements for the sensor is presented in Fig. 3.

For the case A compression forces are applied on both ends of the PVDF sensor. Taking into account the cross-section area a pressure of 300 kPa has been applied on each side. The second case B is when the force is applied perpendicularly along the length of the sensor.

The results of both simulations are shown in Fig. 3 and Fig. 4. The voltage in case A is approx. 1.6V and in case B is 1.7V.

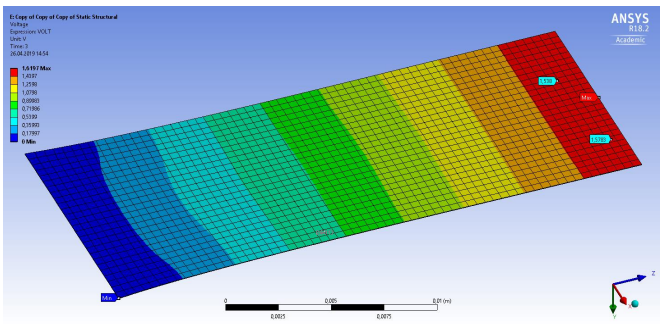

Fig. 3. FEA of the PVDF sensor with compression force applied. Case A.

Additional static analysis was performed to obtain a deflection level for each of the case-studies. Results of this simulation are presented in Fig. 5. Open-circuit voltage computed in FEA was close to the analytical calculations presented in previous subsection.

IV. Analog and Digital Interface

A. Charge amplifier

A charge amplifier (CA) eliminates the effects of the time constants of both the piezo film and connecting cable. An ideal CA is a current operated circuit with zero input impedance,

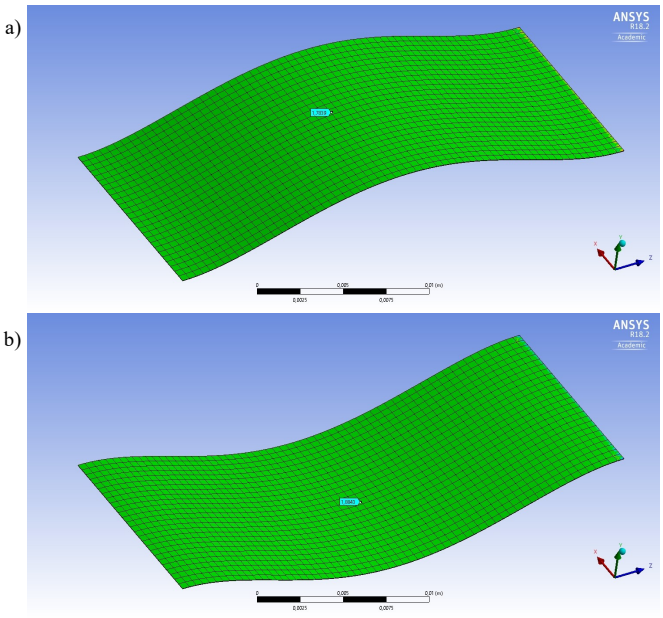

Fig. 4. FEA of the PVDF sensor with bending force applied. Case B.

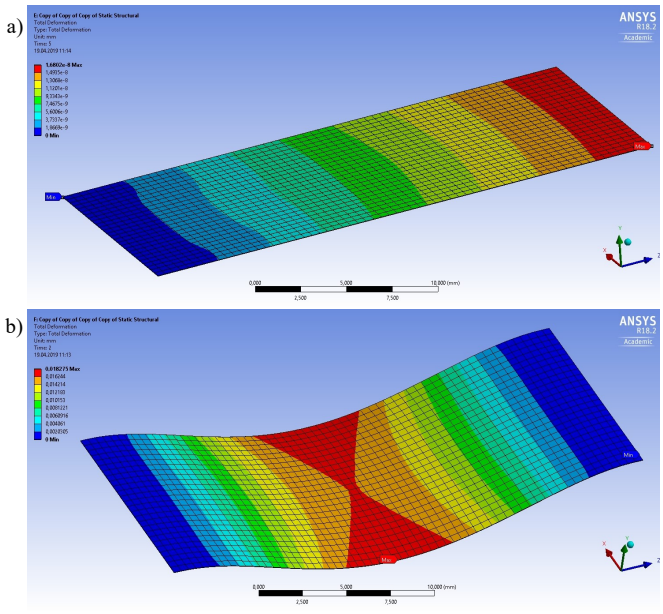

Fig. 5. FEA of deflection level for both case-studies: a) case A- compression forces; b) case B - bending forces.

which results in no voltage being generated across the film. The charge amplifier requires an operational amplifier to have a high input impedance and low bias current. A high input resistance avoids bleed-off of the charge on the feedback capacitor C_F, and low bias current prevents the feedback capacitor from charging and discharging at excessive rates [14].

CA transfers the charge to a reference capacitor and produces an output voltage which is proportional to the charge on feedback capacitor C_F and, respectively, to the input charge;

hence the circuit acts as a charge-to-voltage converter. The output voltage is independent of cable capacitance, therefore longer interconnects between sensors and the electronics can be used. The output voltage of the CA can be calculated as follows:

$$V_{out} = -\frac{q}{C_F} \tag{6}$$

CA sets the low cut-off frequency, f_L:

$$f_L = \frac{1}{2\pi R_F C_F} \tag{7}$$

Low frequency operation of the circuit can be controlled only by adjusting components in the feedback of CA. For low attenuation of respiration and heart beat signals f_L around 0.1 Hz is desirable. In combination with the appropriate level of gain, this fact sets the requirement for the feedback resistor R_F to be in the range of MΩ, while even values in GΩ range are not uncommon. The schematic of CA is shown in Fig. 6

It is good practice to balance the inputs of the op-amp for reduced noise spectrum. However for balancing capacitors (which should be equal to $C_P \parallel C_F$) higher than 300 pF this operation gives smaller impact on noise performance of the amplifier [15]. Another design consideration was feedback resistor R_F in the range of hundreds of MΩ. To avoid using separate high values resistors, which tend to be bulky and pricier, a *T* resistive network (consisting of R_1, R_2 and R_3 resistors) was utilized. This solution, however, may introduce higher noise levels, which could be an issue for greater gain *K* of the circuit. The final values of prototype CA are listed in the Table II.

The operational amplifier is supplied with +5DC, which is fed by a low-cost development board (Arduino Uno). The sensor and the positive input of CA are kept at the potential V_r=*2.5* V. The output voltage V_{out} will swing above and below V_r. This dc offset is later removed in the digital filtering stage. The voltage V_{out} is converted to digital by a 10-bit resolution ADC with sampling frequency $f_s = 79$ Hz within the platform. Digital sensor data is then transferred by a serial communication to the Matlab environment for further signal conditioning with infinite impulse response filters.

TABLE II
PARAMETERS OF THE CHARGE AMPLIFIER.

Name	Final Value
C_F [nF]	10
R_F [Ω]	$2.14{\cdot}10^8$
R_1 [Ω]	$1{\cdot}10^6$
R_2 [Ω]	$1{\cdot}10^5$
R_3 [Ω]	470
V_r [V]	2.5
K [-]	0.14
f_L [Hz]	0.079

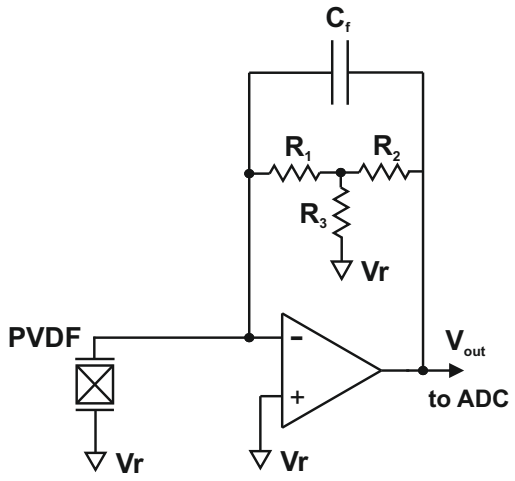

Fig. 6. Charge amplifier adopting signal from PVDF sensor for use in external analog to digital converter.

B. Signal filtering

In order to extract the meaningful respiration and/or heart-beat signals from the sensor's interface, use of filtering was necessary. Authors decided to perform this process on the digital side due to much higher flexibility of DSP methods, available tools and future implementation in hardware such as FPGA. Thus a natural choice was Infinite Impulse Response filter family. On one hand, the main advantage of IIR is less computing power needed for a given filtering characteristics compared to a similar Finite Impulse Response (FIR) filter [16]. Problems with IIR filters, on the other hand, typically arise due to finite-length arithmetic and the presence of feed-back. Transfer function of a second order digital filter can be expressed as follows:

$$H(z) = \frac{b_0 + b_1 z^{-1} + b_2 z^{-2}}{1 - a_1 z^{-1} - a_2 z^{-2}} \tag{8}$$

Where: a_n, b_n are coefficients of the filter. A general 2-nd order IIR filter can be realized with addition and multiplication operations, and known previous output and input states, as can be seen in the difference equation:

$$\begin{aligned} y(n) &= a_1 y(n-1) + a_2 y(n-2) \\ &+ b_0 x(n) + b_1 x(n-1) + b_2 x(n-2) \end{aligned} \tag{9}$$

In order to achieve a better filter characteristics higher orders are needed. Commonly used practice is to adopt a cascade structure of 2-nd order sections:

$$H(z) = H_1(z) H_2(z) ... H_n(z) \tag{10}$$

For the sensor patch located on the abdomen (location *A*) the goal was to capture slow and abnormal (very fast, shallow breathing) respiration signal. For normal breathing, low-pass IIR filter was employed to reduce the noise associated with the charge amplifier electronics or μ-controller board. Butterworth, minimum order design method was used for -3db frequency $f_{pass} = 3$ Hz and attenuation of 60 dB at 5 Hz.

This resulted in 7, 2-nd order sections of the filter. For fast and shallow breathing cycle specification of the Butterworth, low-pass filter was as follows: -3db frequency $f_{pass} = 5$ Hz and attenuation of 60 dB at 10 Hz. This resulted in 5, 2-nd order sections of the filter.

For measurements on the chest (location *B*) the aim was to capture sensor signal containing both respiration and heartbeat data. Two IIR band-pass, Butterworth, minimum order filters were designed to separate the bio-signals from each other and from high frequency noise. For the filtration of respiration data, filter specification was as follows: passband from 0.1 to 0.5 Hz with 2dB ripples, and attenuation for frequencies in the range $0.05 > f > 0.8$Hz of 40dB. The number of sections was 8. For the filtration of heartbeat signal, band-pass filter was designed to meet: passband from 1 to 2 Hz with 2dB ripples, and attenuation for frequencies in the range $0.8 > f > 2.2$ Hz of 40dB. The number of sections was 20.

V. Measurement Results

Measurements were performed with a prototype system consisting of LDT1-028K PVDF sensor connected to an interface circuit. The analog stage of the circuit was a charge amplifier described above, while the digital stage included analog-to-digital converter and an ATmega328 μ-controller. Later, data was sent into Matlab software for digital filtering and FFT analysis. The dominant frequencies extracted from the power spectrum of filtered bio-signals were used to calculate *RR* and *HR*.

A. Location A – abdomen

For the sensor attached to a location *A*, two different tests were performed. Slow breathing for a period of approximately 50s resulted in dominant frequency $f_{rr} = 0.15$ Hz, which corresponded to a RR of 9 bpm (Blue plots in Fig. 7). Second test was an attempt of abnormal respiration cycle with deliberately faster period and shallow nature. This test resulted in frequency $f_{rr} = 1.6$ Hz and RR of 96 bpm (Red plots in Fig. 7). This was unnaturally high value and could not be sustained for long periods of time. Moreover, the test performed were aimed at confirming the concept, i.a. testing the lower frequency limit of CA, not adequately simulating medical conditions.

B. Location B – chest

For the sensor attached to a location *B* resulting voltage signals were of smaller amplitude due to reduced physiological movements of the chest. However, this measurement contained, both, the respiration and heartbeat data. Due to those facts, higher order, band-pass filters were utilized. The unfiltered voltage from analog circuitry (blue trace), filtered respiration signal (red trace), heartbeat signal (black trace) and their respective spectra are presented in Fig. 8.

From it we can calculate the RR of 18 breaths/min ($RR = f_{rr} \cdot 60 = 0.3 \cdot 60$) and the HB of 73.2 beats/min ($HB = f_{hb} \cdot 60 = 1.22 \cdot 60$). The test were performed for calm breathing and no additional physical activity. Different conditions, such as faster respiration and other patient movements, may cause difficulties with separation of RR from HB. This would require more advanced filtering strategy.

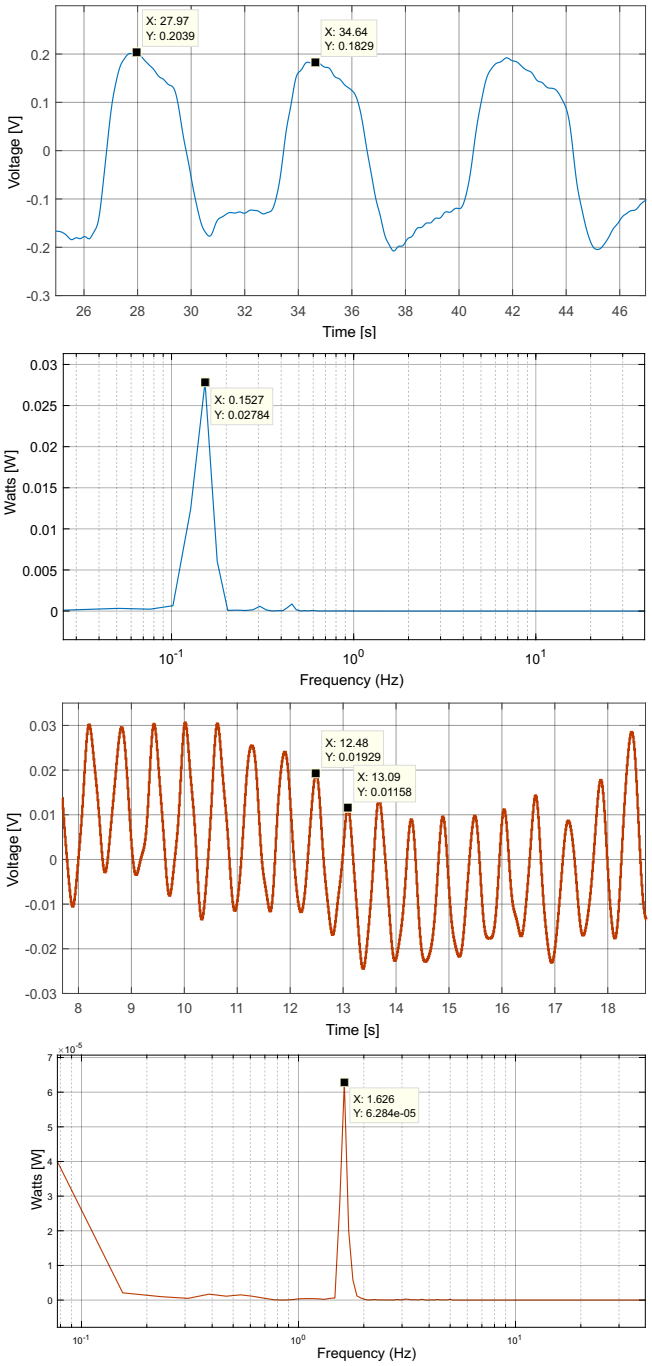

Fig. 7. Measurement results for sensor attached to abdomen. From top to bottom: Voltage output for deep, slow breathing; Spectrum of this signal shows dominant frequency of 0.15 Hz; Voltage output for very fast, shallow breathing; Spectrum of this signal shows dominant frequency of 1.6 Hz.

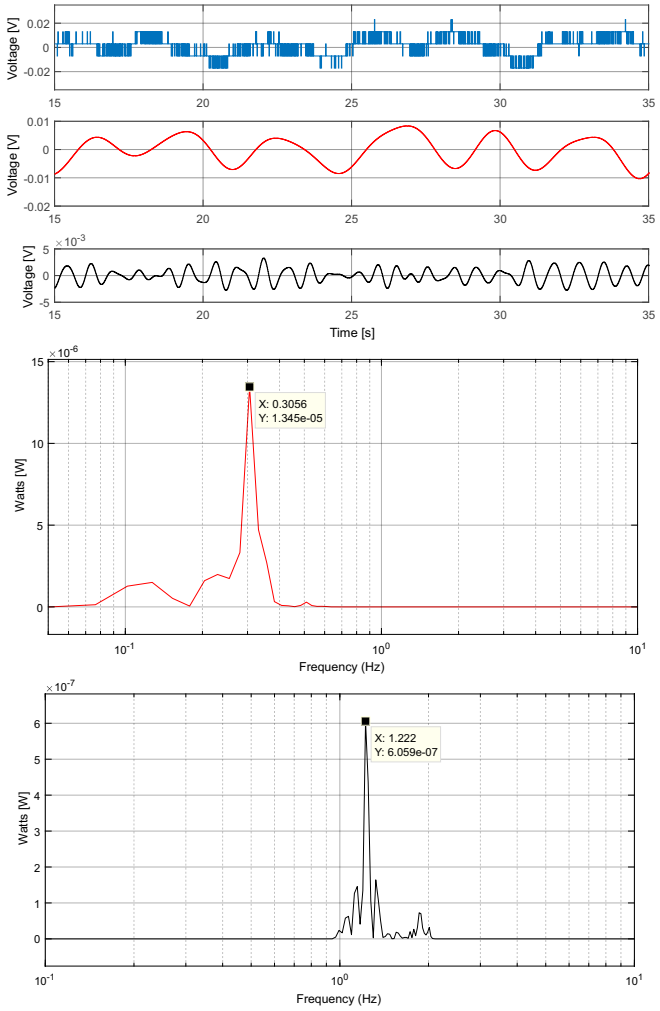

Fig. 8. Measurement results for sensor attached to the chest. From top to bottom: Unfiltered voltage output for normal breathing (blue), band-pass filtered breathing (red) and heart beat signals (black); Respective spectrum of those signals show dominant frequencies of 0.3 Hz (red) for respiration and 1.22 Hz (black) for heartbeat.

VI. Conclusion

The presented low-cost solution enables capturing of respiration rate as well as heartbeat rate without the use of belts or face attachments. This is possible with simple filtering and could be integrated into small package, not affecting the comfort of the patient. Future works may include:

- Implementation of digital signal conditioning in FPGA for more advanced filtering. Problems of motions not related to bio signals or respiration and heartbeat at similar frequencies may be solved with adaptive filtering strategies.

- Packaging of the data and low-power wireless transmission. This aspect is crucial in continuous monitoring, visualization and alerting system using mobile devices.

Measurement in home conditions, which is more natural for the patient, may help to provide longer and more complete registrations of respiration and heart rate. Those, in consequence, may expand the understanding of the breathing variability.

Acknowledgement

Authors express gratitude towards MESCO, an authorized distributor of ANSYS, for granting the Workbench license.

References

[1] M. S. Vijaya, *Piezoelectric Materials and Devices : Applications in Engineering and Medical Sciences*. CRC Press, Apr. 2016.

[2] W. Przyborowski, "Podstawy teorii elektropiezosprzystosci silnikow piezoelektrycznych o kinematyce postepowej i obrotowej," *Biuletyn Wojskowej Akademii Technicznej*, vol. Vol. 67, no. nr 4, 2018.

[3] C.-C. Ma, Y.-H. Huang, and S.-Y. Pan, "Investigation of the transient behavior of a cantilever beam using PVDF sensors," *Sensors (Basel, Switzerland)*, vol. 12, no. 2, pp. 2088–2117, 2012.

[4] Y. Jia, X. Chen, Q. Ni, L. Li, and C. Ju, "Dependence of the Impact Response of Polyvinylidene Fluoride Sensors on Their Supporting Materials' Elasticity," *Sensors (Basel, Switzerland)*, vol. 13, no. 7, pp. 8669–8678, Jul. 2013.

[5] F. Yasuma and J.-I. Hayano, "Respiratory sinus arrhythmia: Why does the heartbeat synchronize with respiratory rhythm?" *Chest*, vol. 125, no. 2, pp. 683–690, Feb. 2004.

[6] R. Sassi, S. Cerutti, F. Lombardi, M. Malik, H. V. Huikuri, C.-K. Peng, G. Schmidt, and Y. Yamamoto, "Advances in heart rate variability signal analysis: Joint position statement by the e-Cardiology ESC Working Group and the European Heart Rhythm Association co-endorsed by the Asia Pacific Heart Rhythm Society," *Europace: European Pacing, Arrhythmias, and Cardiac Electrophysiology: Journal of the Working Groups on Cardiac Pacing, Arrhythmias, and Cardiac Cellular Electrophysiology of the European Society of Cardiology*, vol. 17, no. 9, pp. 1341–1353, Sep. 2015.

[7] R. B. Berry, R. Budhiraja, D. J. Gottlieb, D. Gozal, C. Iber, V. K. Kapur, C. L. Marcus, R. Mehra, S. Parthasarathy, S. F. Quan, S. Redline, K. P. Strohl, S. L. Davidson Ward, M. M. Tangredi, and American Academy of Sleep Medicine, "Rules for scoring respiratory events in sleep: Update of the 2007 AASM Manual for the Scoring of Sleep and Associated Events. Deliberations of the Sleep Apnea Definitions Task Force of the American Academy of Sleep Medicine," *Journal of clinical sleep medicine: JCSM: official publication of the American Academy of Sleep Medicine*, vol. 8, no. 5, pp. 597–619, Oct. 2012.

[8] R. G. Manjunatha, N. Ranjith, Y. V. Meghashree, K. Rajanna, and D. R. Mahapatra, "Identification of different respiratory rate by a piezo polymer based nasal sensor," in *2013 IEEE SENSORS*, Nov. 2013, pp. 1–4.

[9] E. De la Hoya, J. Cota-Ruiz, and R. Gonzalez-Landaeta, "Respiratory Rate Detection by a Time-Based Measurement System," *Revista Mexicana de Ingenieria Biomedica*, vol. 37, pp. 91–99, May 2016.

[10] Y. Xin, C. Guo, X. Qi, H. Tian, X. Li, Q. Dai, S. Wang, and C. Wang, "Wearable and unconstrained systems based on PVDF sensors in physiological signals monitoring: A brief review," *Ferroelectrics*, vol. 500, no. 1, pp. 291–300, Aug. 2016.

[11] G. Chao, X. Shanhong, D. Kai, B. Qiang, and S. Chen, "Design and simulation of miniature vibrating electric field sensors," in *2004 IEEE SENSORS*, Oct. 2004, pp. 1589–1592 vol.3.

[12] Y.-Y. Chiu, W.-Y. Lin, H.-Y. Wang, S.-B. Huang, and M.-H. Wu, "Development of a piezoelectric polyvinylidene fluoride (PVDF) polymer-based sensor patch for simultaneous heartbeat and respiration monitoring," *Sensors and Actuators A: Physical*, vol. 189, pp. 328–334, Jan. 2013.

[13] A. Żak and M. Krawczuk, "A higher order transversely deformable shell-type spectral finite element for dynamic analysis of isotropic structures," *Finite Elements in Analysis and Design*, vol. 142, pp. 17–29, Mar. 2018.

[14] L. Pinna and M. Valle, "Charge Amplifier Design Methodology for PVDF-Based Tactile Sensors," *Journal of Circuits, Systems and Computers*, vol. 22, Sep. 2013.

[15] T. Starecki, "Analog Front-End Circuitry in Piezoelectric and Microphone Detection of Photoacoustic Signals," *International Journal of Thermophysics*, vol. 35, pp. 1–16, Nov. 2014.

[16] C. Mei Wang and W. Cai Xiao, "Second-Order IIR Notch Filter Design and Implementation of Digital Signal Processing System," *Applied Mechanics and Materials*, vol. 347-350, Feb. 2013.